Quasi-Periodic Patterns of Intrinsic Brain Activity in Individuals and their Relationship to Global Signal

Behnaz Yousefi[1], Jaemin Shin[2], Eric H. Schumacher[3], Shella D. Keilholz[4]

[1] Biomedical Engineering, Emory University/Georgia Institute of Technology, 1760 Haygood Dr, HSRB W200, Atlanta, GA 30322 404-727-2433 bzyousefi@gatech.edu

[2] Center for Advanced Brain Imaging, Georgia Institute of Technology, 831 Marietta St NW, Atlanta, Georgia 30318, 404-385-8624 jaemins@gatech.edu

[3] School of Psychology, Georgia Institute of Technology, 654 Cherry Street, JS Coon Bldg R224, Atlanta, Georgia 30332, 404-894-6067 eschu@gatech.edu

[4] Biomedical Engineering, Emory University/Georgia Institute of Technology, 1760 Haygood Dr, HSRB W200, Atlanta, GA 30322 404-727-2433 shella.keilholz@bme.gatech.edu

Abstract

Quasiperiodic patterns (QPPs) as reported by Majeed et al., 2011 are prominent features of the brain's intrinsic activity that involve important large-scale networks (default mode, DMN; task positive, TPN) and are likely to be major contributors to widely used measures of functional connectivity. We examined the variability of these patterns in 470 individuals from the Human Connectome Project resting state functional MRI dataset. The QPPs from individuals can be coarsely categorized into two types: one where strong anti-correlation between the DMN and TPN is present, and another without this anti-correlation. QPP type could be predicted by an individual's global signal, with higher global signal corresponding to QPPs without anti-correlation. After global signal regression, all QPPs showed strong anti-correlation between DMN and TPN. QPP occurrence and type was similar between a subgroup of individuals with extremely low motion and the rest of the sample, which shows that motion is not a major contributor to the QPPs. QPP occurrence only weakly correlates with the estimate of slow respiratory-induced fMRI signal fluctuations, an indication that physiological noise is not the primary source of the QPP. QPPs were more similar for the same subjects scanned on different days than for different subjects. These results provide the first assessment of the variability in individual QPPs and their relationship to physiological parameters.

Introduction

Spontaneous fluctuations in the blood oxygenation level dependent (BOLD) MRI signal attributed to intrinsic brain activity exhibit varied dynamic patterns that have been described as time-varying correlation (Chang and Glover 2010; Allen et al., 2012; Keilholz et al., 2013), sparse patterns of localized spontaneous activations (Petridou et al., 2013; Caballero Gaudes et al., 2013), or co-occurring activity (Liu and Duyn 2013; Chen et al., 2015), and repeated spatiotemporal patterns (Majeed et al., 2011; Kiviniemi et al. 2016; also see Preti et al., 2016 for a recent review on varied dynamic patterns). Quasi-periodic patterns (QPPs) fall into the last category and consist of a reproducible pattern of spatial changes that repeat over time, exhibiting alternation of high and low activity in particular areas and propagation of activity along the cortex. QPPs were first observed in anesthetized rats as a bilateral

propagation of high activity from lateral to medial cortical areas, followed by an echoing propagation of low activity (Majeed et al., 2009). Majeed and colleagues (2011) subsequently developed a pattern-finding algorithm to identify QPPs in humans, which involved alternating high and low activity in default mode (DMN) and task positive (TPN) networks. Animal and human studies have shown that QPPs are linked to infra-slow electrical activity (Pan et al., 2013; Thompson et al., 2014a, 2014b, 2015; Keilholz 2014; Grooms et al., 2017) and represent a different type of activity than the higher frequency activity tied to time-varying BOLD correlation between areas (Thompson et al., 2015; Keilholz et al., 2016). Infra-slow electrical activity is one of the best candidates for the coordinating mechanisms within and between brain's large-scale networks (see discussion in Thompson et al., 2014a, 2014b for literature review), and BOLD QPPs can reflect aspects of such mechanisms.

The QPP algorithm is a correlation-based iterative algorithm that identifies a recurring spatiotemporal template during a functional MRI scan (Majeed et al., 2011). First, a segment of a preset number of consecutive timepoints is selected based on a random starting point. Sliding correlation of this segment with the functional scan is calculated, timepoints corresponding to local maxima above a preset threshold are selected, and segments of the scan starting at those timepoints are averaged together with the original segment to create a template. The sliding correlation is then repeated with the template in place of the initial random segment and the process repeats until the template exhibits negligible change between iterations. Thus far, the QPP method has been used with multiple randomly selected starting timepoints followed by a hierarchical clustering to select the most representative QPP. It has typically been applied to concatenated scans from all subjects, meaning that a single template is derived for the entire group, with variable levels of contribution across subjects.

To examine variability in the QPPs at the individual level, we made two modifications to the QPP method that increased its robustness: 1) segments starting at all timepoints of each scan are used to create templates rather than using a limited number of random timepoints, and 2) a customized criterion for the selection of the most representative QPP is introduced based on maximizing the template's correlation with functional scan and the template's periodicity. The modified algorithm was applied to resting state functional MRI data from the Human Connectome Project (HCP) (Van Essen et al., 2013; Glasser et al., 2016a) at the individual level. To examine the effects of motion, analysis was performed on a subgroup of 40 individuals with extremely low motion and compared to 470 subjects with more moderate levels.

Large-scale patterns such as QPPs are likely to contribute to the global signal, so analysis was performed before and after global signal regression. Slow variations in respiration depth and rate have been shown to correlate with variations in the global signal (Power et al., 2017; Liu et al., 2017; Keilholz et al., 2016; Chang and Glover 2009) and with variations in the default mode network (Birn et al., 2006 and 2008), so the relationship between respiration and QPPs was also examined. To compare the levels of variability within individuals to variability across individuals, the HCP resting state scans acquired over two subsequent days were analyzed separately. This report provides the first examination of individual variability in QPPs and provides further support that the patterns reflect neural activity rather than physiological noise or motion. Because QPPs contribute substantially to functional connectivity, especially in the default mode network, a better understanding of their properties and sources can

provide insight into the connectivity differences underlying different behavioral states and traits and connectivity changes associated with neurological and psychiatric disorders.

Method

Data and preprocessing. Minimally preprocessed grayordinate and FIX de-noised resting state scans were downloaded from the Human Connectome Project S900 release (Glasser et al., 2013; Glasser et al., 2016a). To minimize potential contributions from motion, the head motion data from the 820 HCP subjects with four complete resting state scans was inspected and 40 subjects with mean frame-wise displacement (FD; Power et al., 2014) less than 0.12mm per scan for all four scans were selected for initial analysis (designated "low movers" in the text). After QPPs proved detectable and robust at the individual level in this group of high quality data, the selection criterion was relaxed to include 470 subjects with temporal ratio of (FD>0.2mm) less than 0.4 (FD-spikes < %40) per scan for all the four scans (the "low-moderate movers" (see **Fig. S1a**; mean FD < 0.2mm; note that all low movers were included among the low-moderate movers). Previous work that has specifically examined motion in the HCP dataset used spikes in temporal Derivative then rms VARiance over elements (DVARS or DV) in addition to FD to identify high motion timepoints (Burgess et al., 2016; Siegel et al. 2016). Therefore, we examined DV as well (Fig. S1a and **S1b**). In the initial analysis of the 40 low movers, QPP detection was performed using the timeseries of all ~92K cortical vertices and subcortical voxels. To maintain practical computation times for the larger group of low-moderate movers with our modified approach to QPP detection, the spatial dimension was reduced to 360 cortical parcels (Glasser et al., 2016b) by averaging vertices' timeseries across each parcel and normalizing the z-scores of each parcel's timeseries.

The timeseries of each vertex/voxel per scan underwent the following processing steps: 1) demeaning 2) band pass filtering (Butterworth, forth order, 1dB cutoff frequencies: 0.01 and 0.1Hz) using Matlab fdesign and filtfilt functions (424 zeros pads were inserted at both ends of each 1200-timepoint scans before filtering and were removed afterwards to minimize transient effects), and 3) normalization by their own standard deviations. For the initial analysis, no global signal regression was performed.

Modified QPP detection method. The original approach described by Majeed et al., to identify QPPs involved choosing a limited number of randomly selected starting timepoints, running the main algorithm and finding the templates corresponding to those starting timepoints, using hierarchical clustering on those templates, and finally selecting the template that has the maximum average correlation with the rest of the templates in the biggest cluster. However, some starting timepoints result in a template that has a low correlation with the functional scan or does not occur often. Other starting timepoints may pick up the same template but at different phases. To examine the full potential of the main algorithm, a computationally efficient Matlab script was developed to inspect the templates resulting from all the timepoints. It exactly replicated the main algorithm, keeping all free parameters the same (correlation threshold of 0.1 for the first 3 iterations and 0.2 for the rest, maximum iteration of 20). QPPs in humans are approximately 20s long (Majeed et al., 2011); for this study, the window length (template duration) was set to 30 timepoints (21.6s). Four scans were concatenated for each subject and the new QPP script inspected every timepoint ($4\times(1200-30+1)=4684$).

Fig. 1 demonstrates the use of all timepoints to identify templates: in **Fig. 1a**, the time course of correlation for a template corresponding to a single starting timepoint is shown for one individual. In **Fig. 1b**, timepoints corresponding to supra-threshold local maxima of such correlation are plotted in the vertical axis for each starting time point, and the value of correlation is indicated by color. When all timepoints are considered as starting timepoints, considerable redundancy results (sequential starting timepoints or those ~30 timepoints apart are essentially the same template) and templates from some timepoints exhibit low correlation or periodicity. Hence, for the template resulting from each timepoint, values of its correlation at supra-threshold local maxima were summed and the template with the highest sum was designated as the most representative QPP. Selected in this way, the most representative QPP is guaranteed to have high correlation and large numbers of occurrences relative to other templates.

Characterizing the spatial extent of the anti-correlation within the duration of a QPP. One of the most prominent features previously noted in the QPP is that patterns of activity are 180 degrees out of phase (i.e., anti-correlated) for regions of the DMN and TPN. To test for and characterize this feature, each of 14 parcels in left posterior cingulate cortex (LPCC) was taken as a seed, one at a time, and the histogram of Pearson correlation values between the 30-timepoint template timeseries of each seed with all 360 parcels was calculated with bin centers -0.9:0.2:0.9. The histogram with maximum first bin (number of parcels with correlation between -1 and -0.8) was selected for each subject. In the case of zero count for the first bin for all seeds, the timeseries of all seeds were averaged and again a histogram of Pearson correlation values with all 360 parcels was calculated with the same bin centers. (Note that for the 40 low movers, the procedure above was done after reducing their QPP dimension to 360×30 by averaging across each parcel; for 470 low-moderate movers, QPP dimension was already 360×30 since the QPP analysis was performed parcel-wise.)

Relationship between QPPs and global signal. Because large, spatially coherent patterns such as the QPP may contribute to the global signal, the relationship between QPPs and the global signal was explored as one of the central pillars of the current work. Because the analysis was performed in grayordinates, we used the cortical and subcortical signal (the average of the timeseries of cortical vertices and subcortical voxels) as an approximation for the global signal, which previous studies have shown originates primarily in the gray matter (Glasser et al., 2016a; Power et al., 2017). Furthermore, in the case of the 470 low-moderate movers, the relation with the cortical signal (the average of the timeseries of cortical vertices) was also explored since their QPP analysis was performed using only cortical parcel-wise timeseries. The total cortical and subcortical signal is highly correlated with the cortical signal (r=0.99; **Fig. S2**).Throughout this article, we have used the term global signal in general statements in place of cortical and subcortical signal or cortical signal.

The following approaches were taken to explore the relationship between QPPs and the global signal:

1) The values of the first and the last bins of the correlation histograms described above, which reveal the spatial extent of strong negative and strong positive correlation in the QPPs, were plotted against the root mean square (rms) of the global signal. Suggested by a clear visual division in the values of the last bin, QPPs were clustered into two groups (two QPP types) using Kmeans, with the values of the last

bin being the input. The rms of the global signals were compared between groups using an unpaired t-test.

2) Global signal was regressed and the QPP analysis was repeated. For global signal regression, the timeseries of each vertex underwent only the first two steps of the preprocessing, then global signal was calculated by averaging across all vertices. General linear modeling (GLM) was performed with the global signal as the regressor. The residual timeseries were averaged across each parcel, and the parcels' timeseries were z-scored. The correlation histograms were then calculated again to determine the effect on the spatial extent of strong positive and negative correlation.

3) The QPP of each subject was convolved with its corresponding correlation time course (QPP⊗C) and the result was cross-correlated with the global signal (allowed lag: -20 to 20 timepoints; throughout this work, the maximum of the absolute value of cross-correlation and the corresponding lag are reported). The goal of this procedure was to determine whether QPP occurrence coincided with timepoint-by-timepoint fluctuations of the global signal. The temporal pattern of the QPP is different for each parcel (or voxel), so for each subject, we selected the parcel whose raw timeseries had the highest correlation with the global signal (ROI_{GS}). To build a null distribution for cross-correlation values, phase-randomized timeseries were made out of QPP⊗C@ROI_{GS} and the global signal as described in Majeed et al., 2011 for each subject. The phase randomized time series were then cross-correlated (allowed lag: -20 to 20 timepoints), and the Kolmogorov-Smirnov (KS) test was adopted to compare the distributions from the real and phase-randomized data.

Relationship between QPPs and respiration. Slow variations (<0.1Hz) in respiration rate and depth are known to correlate with fluctuations of the global signal (Power et al., 2017; Liu et al., 2017; Keilholz et al., 2016; Chang and Glover 2009) and with BOLD fluctuations in the DMN (Birn et al., 2006). To examine the relation between QPPs and slow respiratory-induced BOLD fluctuations, the respiratory belt traces of the 470 low-moderate movers were despiked (Matlab medfilt1), lowpass filtered (Matlab filtfilt and fir1, order 40, as in RetroTS.m suggested by Power et al., 2017), amplitude clipped to ±2.5 standard deviation from mean (to remove outliers not fixed by despiking), and amplitude rescaled to 0-100, as in RetroTS.m (**Fig. S3a**). Each preprocessed trace was visually inspected; 423 subjects had acceptable quality respiration data for all four scans.

Respiratory Variation (RV), defined as the standard deviation of the respiratory waveform in a sliding window of 7.2s (10 timepoints, ~two respiratory cycles) centered around each fMRI scan timepoint (Chang et al., 2009), was then calculated for each scan. HCP respiration data often has short lapses causing spikes in RV; therefore, based on the histogram of the standard deviation of RV (std RV), for further respiration related analyses, only subjects whose std RV for all scans were within three standard deviations above the median were included (403 subjects; **Fig. S3b**).

The values of the first and the last bin of the correlation histogram of each QPP (corresponding to the spatial extent of strong negative and positive correlations) were plotted against the average of std RV across four scans. The average of std RVs across four scans was compared between groups with the two QPP types using an unpaired t-test. In addition, the Respiratory Response Function (RRF) as described in Birn et al., 2008 and Chang and Glover 2009 was convolved with RV (RRF⊗RV) to build the estimate of

respiratory-induced signal fluctuations. QPPs were convolved with their corresponding correlations (QPP⊗C) and cross-correlation between RRF⊗RV and QPP⊗C (allowed timepoint shifts: -20 to 20) was calculated. This was an attempt to inspect QPP occurrence with respiratory-induced signal fluctuations in a timepoint-by-timepoint manner. Since QPP⊗C is parcel dependant, the parcel whose raw timeseries had the highest cross-correlation with the RRF⊗RV (ROI_{RV}) for each subject was selected. A null distribution was built by applying a similar process to phase-randomized timeseries made from the original ones and the KS test was used to compare distributions.

Metrics for QPP correlation and periodicity. To obtain a single value that describes the overall strength of the QPP during a scan, we used the median of QPP correlation with the scan at supra-threshold local maxima (Fig. 1). Similarly, the median of the time between successive supra-threshold local maxima indicates how often a QPP occurs throughout the functional scan (QPP periodicity). Hence, these metrics were calculated for 470 low-moderate movers. The frequency characteristics of the QPP correlation timecourse were also examined using the Fourier Transform.

Comparing QPPs between sessions. The four HCP resting state scans were acquired over two subsequent days (two ~15mins back-to-back scans per day), providing an opportunity to examine the relationship between QPPs in the same individual on separate days; therefore, QPP analysis was performed separately on the concatenated scans from each day. QPPs were identified based on the modified method introduced earlier, and histograms of correlation with LPCC were calculated for each QPP. As before, the values of the last bin were used as the input to cluster the QPPs of all subjects of both days using Kmeans. QPP type, its median correlation and its periodicity were compared between the two days.

Calculating the correlation between the most representative QPPs of separate days requires both templates to have the same phase; for instance, both start around zero at timepoint 1 and reach their maximum during the first half of their cycle rather than one reaching its minimum in the first half and maximum in the second half. In order to phase-adjust a representative QPP, its correlation time course was cross-correlated with that of all other templates (corresponding to all other inspected starting timepoints). Templates with values greater than 0.9 were kept (they are similar to the most representative QPP but can have different phases) and sorted based on their sum of correlation at supra-threshold local maxima. The first template whose left early visual area (parcel 184) had a value near zero at timepoint 1 and its maximum occurred before timepoint 15 was designated as the phase-adjusted QPP. After inspecting all 470 subjects, we decided to add two more strict conditions (the value of the first three timepoints must be more than zero and the value of maximum must be more than the minimum) which achieved near-perfect phase-adjustment at the cost of reducing the number of subjects to 196. For the within subject comparisons, the 2D spatio-temporal arrays of phase-adjusted QPPs of each day were flattened to 1D, and their Pearson correlations were calculated. For between subject comparisons, phase-adjusted QPP of both days from each subject were correlated to those of all other subjects (196×195×4 comparisons) using the same procedure.

Basic demographics: Out of 470 low-moderate movers, 241 are female (out of 820 HCP with four complete resting state scans, 453 are female). There are 124 twins (62 pair, 31 monozygotic), 196 two-sibling individuals (98 pair, twin or not), 105 three-sibling and 20 four-sibling individuals (two of 3 or 4

siblings might be twin); only 149 individuals have no siblings. The 470 low-moderate movers' median age is 28 with standard deviation of 3.6 and range of 22-36 (median age of all 820 subjects is 29, standard deviation of 3.7 and range: 22-37).

Results

Despite the use of the modified method for identifying QPPs, the overall spatial and temporal distribution of activity was similar to that described in Majeed et al., 2011. In all cases, activation and deactivation of areas belonging to the DMN occurred. For some individuals, the TPN exhibited anti-correlation with the DMN, while for other individuals, only positively correlated activity was observed in most areas. After global signal regression, however, the QPPS become more similar in that anti-correlation between the DMN and TPN was observed for all individuals. While all analysis was performed on the individual basis for this manuscript, the resulting spatiotemporal patterns were in good agreement with previous work that calculated QPPs on a group basis (Majeed et al., 2011; Kiviniemi et al. 2016).

Fig. 2a shows QPPs from two representative subjects out of the 40 low movers before global signal regression (**Videos 1 and 2** show all 30 timepoints and **Fig. 2b** shows the parcel-wise format). The QPP from the first subject exhibits clear anti-correlation between the activity levels in the DMN and TPN (anti-correlated type of QPP). In the second subject, however, most of the brain activates, with only a few time points showing anti-correlation (most-correlated type of QPP). The histograms of correlations with the LPCC for the two QPPs from the same subjects are plotted in **Fig. 3a**. Within subject 1's QPP, ~40% of ROIs are anti-correlated with LPCC between -1 and -0.8 while within subject 7's QPP, no ROI is anti-correlated with LPCC and %75 of the ROIs have a correlation value greater than 0.8 (this difference is clearly demonstrated in the correlation maps in **Fig. S4a**). **Fig. S4b** shows histograms of correlations within the QPPs for all 40 low movers. It is notable that for some individuals, strong anti-correlated activity appears, while for others, most areas are strongly correlated. **Fig. 3b**, in which 40 low movers are sorted based on the percentage of ROIs correlated<-0.8 with the LPCC (left) or **re**sorted based on the percentage of ROIs correlated>0.8 with LPCC (right), summarizes this feature. The clear separation into two groups of data-points in the right part of Fig. 3b provides further evidence that QPPs should be coarsely categorized into two types (color indicates QPP type).

The widespread involvement of brain areas in the QPPs encouraged us to seek a relationship with the global signal. We plotted the percentage of ROIs with strong negative and positive correlations against the root mean square (rms) of the global signal in **Fig. 3c**. The lower the rms of the global signal, the larger the spatial extent of strong anti-correlations within a QPP, and the higher the rms of global signal, the larger the spatial extent of strong positive correlations within a QPP. The rms of global signal is significantly different between the two QPP types (medians: 0.16 and 0.22, p:2e-4; see whisker plot in **Fig. S4c**).

Similar results, summarized in **Fig. 3d and 3e,** were seen after the pool of subjects was expanded to include individuals with low to moderate levels of motion and analysis was performed on a parcel-wise rather than voxel-wise basis. The rms of the global signal is significantly different between two groups

(medians: 0.21 and 0.27, p:7.3e-22, **Fig. S4d)**. The number of subjects with strong negative and positive correlations for each ROI are plotted in **Fig. 3g**. As expected, most ROIs with strong anti-correlation belong to non-DMN networks and most ROIs with strong correlation belong to the DMN.

The spatial extent of strong negative and positive correlations within a QPP were plotted versus motion metrics for low movers (**Fig. S5a**) and low-moderate movers (**Fig. S5b and S5c**). Neither of the FD metrics was significantly different between groups with different QPP types; however, the DV metric was slightly although significantly higher in individuals with the most-correlated type of QPP (medians: %8 versus %9, p:3e-4. These findings show that low to moderate levels of motion have minimal impact on the QPP. While higher levels of global signal reduce the amount of anti-correlation observed between the DMN and TPN, the relationship between the global signal and the QPP is not tied to motion but rather to some other aspect of the global signal.

After global signal regression, all 470 subjects showed strong anti-correlations within their QPPs (**Fig. 3f**) in areas belonging to non-DMN networks (**Fig. 3h**). **Fig. 2c** shows QPPs of the same two subjects in Fig. 2a, but after global signal regression (**Videos 3 and 4** show all 30 timepoints and **Fig. 2d** shows the parcel-wise format). Anti-correlated activity still exists in subject 1 and is now observed in subject 7. Global signal regression makes the detected QPPs more homogeneous across subjects in terms of the spatial extent of strong negative and positive correlation.

To determine whether the occurrence of QPPs coincides with global signal fluctuations in a timepoint-by-timepoint manner, we convolved the QPP of each of the 470 low-moderate movers with its template correlation timecourse. Because the strength of the QPP varies across parcels, for each subject, we considered QPP⊗C at the parcel whose raw timeseries had the highest correlation with the global signal (ROI_{GS}). We cross-correlated this timeseries with the global signal (allowed lag: -20 to 20 timepoints). **Fig. S6a** shows the distribution of the results. The median is 0.79 and it is significantly higher than the null, indicating that the QPP does often coincide with the global signal fluctuations in a timepoint-by-timepoint manner with small time-shifts. Moreover, the higher the rms of the global signal, the stronger this coincidence. **Fig. S6b** shows the number of subjects exhibiting the highest correlation with the global signal for each parcel; as expected, primary and early visual, somato-motor and auditory areas are the most correlated with the global signal in agreement with (Glasser et al., 2016) and (Power et al., 2017). In addition to taking QPP⊗C at ROI_{GS}, three alternatives were tested:(i) selecting parcel 184, Left Early Visual Area, for all subjects, since this was the parcel with the highest correlation with the global signal overall (**Fig. S6d**), (ii) selecting the parcel at which cross-correlation of QPP⊗C and the global signal was maximum (**Fig. S6f**), and (iii) averaging QPP⊗C across parcels and cross-correlating that with the global signal (**Fig. S6e**). Results were similar for all three approaches.

Fig. 4a shows the rms of the global signal plotted against the standard deviation of respiratory variation (RV). Fluctuations in the global signal are positively correlated with respiratory variations, well in line with Power et al., 2017 where at low motion timepoints, this correlation was shown to be ~0.5. The spatial extent of strong negative or positive correlations within a QPP is solidly predicted by rms of the global signal; hence, they should also be related to respiratory variations. As expected, individuals with the anti-correlated QPP type have slightly, but significantly, lower RV variation compared to those with most-correlated QPP type (**Fig. S7**).

To determine whether the occurrence of QPPs coincides with slow respiratory-induced signal fluctuations, the Respiratory Response Function (RRF), shown in **Fig. S8a**, was convolved with RV (RRF⊗RV) and QPP was convolved with its correlation timecourse (QPP⊗C) from ROI_{RV} (the parcel whose raw timeseries had the highest cross-correlation with RRF⊗RV), then the two were cross-correlated. **Fig. 4b** shows the distribution of the results (median 0.31, range: 0.01-0.86, median of the corresponding lags: 6 (**Fig. S8b**)). The correlation is significantly higher than null (median 0.12, range 0.01-0.48, with uniformly spread corresponding lags; p_{KStest}=1.4e-7). In other words, QPPs weakly yet significantly coincide with respiratory-induced signal fluctuations when time-shifts are compensated, and the higher the rms of the global signal, the higher this coincidence (**Fig. 4c**). Comparing Fig. 4 and Fig. S6, it is obvious that coincidence of QPP with the global signal fluctuations is far stronger than its coincidence with respiratory-induced signal fluctuations. The lag for maximal correlation corresponds to a forward shift of the QPP⊗C@ROI_{RV}, and is roughly in accord with Birn et al., 2008 that in the resting state, ~10s backward shifts of RVT⊗RRF results in the best fit to BOLD signal fluctuations.

Fig. S9a shows the ROI_{RV} count map (number of subjects per parcel). Primary areas for auditory, visual, and somato-motor have the highest cross-correlation with the estimate of respiratory-induced signal fluctuations. It is important to note that as mentioned in Power et al., 2017, we also do not observe the prominent respiratory effects in default regions which were reported in Birn et al., 2006, but rather in the neighboring areas. Fig. S9a also shows the values of cross-correlations corresponding to ROI_{RV} which act as a basis for Fig. 6b and 6c: their distribution with median of 0.42 is significantly different from null (median: 0.31, p_{KStest}:6.3e-4), and the higher the rms of global signal, the higher the cross-correlation values. **Fig. S9b** is similar to Fig. S9a but after global signal regression; all cross-correlation values decrease but remain significantly different from null (median of 0.32 versus 0.29). Primary somato-motor, visual and auditory areas have the highest cross-correlation values, and again there is not a prominent involvement of the default mode network. As shown in **Fig. S9c**, after GSR, coincidence of QPPs and respiratory induced signal fluctuation decreases (median: 0.18), yet remains significantly different from null (median:0.11, p_{KStest}=0.001).

How correlated is the QPP with the functional scan and how often does it occur? The answer can be obtained by inspecting the correlation time course for the QPP and the scan. **Fig. 5a** shows such time courses for the two representative subjects in Fig. 2. Subject1's QPP (anti-correlated type), correlates less with subject1's functional scan as opposed to subject7's QPP (most-correlated type). Also, subject1's QPP occurs less often, with more variability relative to that of Subject7's. For all 470 subjects, the median of QPP correlation at the supra-threshold maxima was 0.35 and the median of the time between successive maxima was 26 s (**Fig. 5b**).

Fig. 5c shows values of Fig. 5b versus rms of global signal, the predictor of strong negative or positive correlations within a QPP. High rms of the global signal corresponds to high correlation and periodicity, meaning most-correlated type QPP correlates relatively more with the functional scan and occurs more often. Low rms of global signal corresponds to low correlation and periodicity, meaning, anti-correlated type QPP correlates relatively less with functional scan and occurs relatively less often. After global signal regression, where all QPPs have strong anti-correlation within them, correlations and periodicities

decrease (**Fig. 5d**, medians:0.31 and 32s). This behavior was expected since after GSR all QPPs become similar to the anti-correlated QPP type before GSR.

To demonstrate the quasi-periodic nature of the QPPs, we plotted the average Fourier transform of all individuals' QPP correlation time courses in the frequency domain as shown in **Fig. 6**. A broad peak at ~0.03Hz (~30s) provides evidence of the quasiperiodic nature of the pattern.

To examine the relationship between QPPs of the same individual on subsequent days, QPP analysis was performed separately on the concatenated scans of each day. The QPP type remains largely the same across two days (**Fig. 7a**): out of the 245 individuals with the anti-correlated type QPP on day 1, 178 (~%73) exhibit the same type on day 2, and out of the 225 individuals with most-correlated type QPP on day 1, 130 (~%58) exhibit the same type on day 2). The rms of the global signal, which predicts QPP type, is highly correlated between days (r=0.79, **Fig. 7b**), suggesting a very interesting point that global signal fluctuation can be regarded as a trait, in addition to reflecting brain states (Wong et al., 2013). Also note that the standard deviation of Respiration Variation which is correlated with global signal (r=0.59, Fig. 6a) is reasonably correlated between days (r=0.6, **Fig. S10a**). QPP correlation and periodicity are collectively reflected in the sum of correlation at supra-threshold local maxima which is reasonably correlated between days (r=0.61, **Fig. 7c**). Both the median of QPP correlation at supra-threshold maxima and the median of the time between successive maxima remain correlated between days (r=0.43 and 0.44, **Fig. S10b**). QPP correlation and periodicity are still correlated across days after global signal regression (**Fig. S10c**) although the correlation values decrease, suggesting that these metrics could potentially be recognized as traits independent of the global signal. **Fig. 7d** shows that phase-adjusted QPPs, derived based on the procedure explained in the methods section, are significantly more correlated between days within subjects (median:0.73) than between subjects (median of 0.56; p_{KStest}:1.4e-13). This finding is unchanged by global signal regression, although medians are reduced (**Fig. S10d**, within subject: 0.44, between subject:0.28, p_{KStest}:3.4e-6).

Out of 233 individuals with anti-correlated type QPP, 148 are female (~%63.5) and out of those with most-correlated type QPP, %60.8 are male. Out of 31 monozygotic twins, 20 have the same QPP type (%64.5); this percentage is %61.3 for 31 non-monozygotic twins. Out of 196 two-siblings individuals (twin or not) %46 have the same QPP type; this percentage is %29 for 105 three-sibling individuals and %20 for 20 four-sibling individuals (two of 3 or 4 might be twins). There is no age difference between group of individuals with two different QPP types (both medians are 28, p=0.85).

Discussion

Summary

In order to perform the first examination of the variability in QPPs across individuals, we developed a robust version of the pattern-finding method that does not depend upon a randomly-chosen starting point. Applying this method to ~500 individuals, we found that QPPs fall into two major categories prior to global signal correction and that these categories are closely linked to the overall level of global signal. After global signal regression, QPPs become remarkably similar in their spatial extent of strong

positive or negative correlation, strength and timing across individuals. The QPPs do not appear to result from motion or respiration, providing further evidence of a neuro-physiological source. Between subsequent days, QPP type, strength and periodicity are reasonably correlated and the pattern itself is somewhat individual-specific.

Potential sources and functional significance of QPPs

BOLD-based QPPs are correlated with electrical intrinsic brain activity in the infra-slow (<0.1Hz) frequency range (Pan et al., 2013; Thompson et al., 2014a, 2014b, 2015; Keilholz 2014; Grooms et al., 2017). The infraslow electrical signals themselves are still poorly understood but may arise from coordinated interactions between neurons, glia, and the vasculature (see the thorough review in Keilholz et al., 2016 and the speculation on the effect of vascular structure in Thompson et al., 2014a). Like traditional BOLD-based networks of functional connectivity, QPPs have been observed in mice (Belloy et al., 2017), rats (Pan et al., 2013; Thompson et al., 2014a, 2014b; Magnuson et al., 2010), monkeys (Abbas et al., 2016a), and humans (Majeed et al., 2011; Kiviniemi et al., 2016), in states ranging from deeply anesthetized to awake. This suggests that they represent a fundamental aspect of the brain's functional organization.

The involvement of the DMN and TPN further suggests that QPPs may be linked to attention or vigilance. The DMN is defined by (i) deactivation during tasks requiring attention to the external environment, and (ii) activation during internally focused and self-referential tasks (Buckner et al., 2008). The TPN is defined as areas that co-activate during tasks requiring externally focused attention. It follows that the DMN and TPN tend to be anti-correlated (Fox et al., 2005; Murphy and Fox 2016). One can further speculate, based on the definitions of the two networks, that the activity levels in each network prior to a task could influence subsequent activity when a task commences, hence predicting measures of behavioral-level performance. Numerous works support this hypothesis (see Rosenberg et al., 2016; Tavor et al., 2016; Smith et al., 2015; Cole et al., 2014; Schultz and Cole 2016). In addition to predicting cognitive traits, a preliminary QPP analysis during a psychomotor vigilance task shows that the phase of the QPP predicts reaction time and can therefore reflect varying cognitive states even within an individual (Abbas et al., 2016b).

Moreover, because numerous neurological and psychiatric disorders exhibit alterations in the DMN in particular (see Broyd et al., 2008 for a comprehensive review), it is plausible that some of these changes may reflect alterations in the QPP. By revealing the course of activation and deactivation of DMN, QPP has the potential to add to our basic cognitive science or improve diagnosis and treatment assessment in mental disorders and neuro-pathological diseases.

QPPs and physiological rhythms

Physiological noise is known to contribute spatially-structured noise into functional connectivity measurements and could conceivably contribute to the large-scale, repetitive patterns observed in the QPPs. Slow variations in respiration depth and rate give rise to fluctuations in the arterial level of CO_2, a potent vasodilator, causing variations in cerebral blood flow and oxygenation (Birn et al., 2006; Chang et al., 2009). These respiratory-induced fluctuations in cerebral blood oxygenation can potentially modulate brain neuronal activity (Moore and Cao 2008; also Power et al., 2017 and Murphy et al.,

2013). Moreover, whether generated by the volition of the subject or not, they might have behavioral implications, e.g., a few deep breaths cause global brain deactivation and feel calming (or see Vlemincx et al., 2013a and 2013b). While QPPs and respiratory variations were correlated, the relationship is not strong enough to explain the existence of the QPP.

In Power et al. 2017, Respiration Volume per unit Time (RVT), introduced by Birn et al., 2006, explained more variation of the global signal compared to RV, so we calculated RVT as well (procedure described in **Fig. S11a**). RV and RVT are correlated (**Fig. S11b**) and both capture respiration variation in rate and depth. The rms of global signal is correlated with standard deviation of RVT (r:0.32, **Fig. S11c**), but the correlation is lower than for RV (r:0.59). In the process of finding ROI_{RVT} , the parcel whose raw timeseries had the highest cross-correlation with RRF⊗RVT, we realized cross-correlation values were very weakly significantly different from null (**Fig. S11e**) and did not pursue the examination of QPP coincidence with RVT-based respiratory-induced signal fluctuations.

Heart beat (rate and contractility) is tightly coupled with respiration (rate and depth) in both fast and slow varying regimes (Power et al., 2017; Chang et al., 2009). Including both processes obviously would have more explanatory power (Chang et al., 2009), yet is unlikely to have a major effect on the correlation with the QPP. Furthermore, Kiviniemi et al., 2016 utilized the QPP algorithm to examine processes explicitly associated with cardiac pulsation and respiration in Magnetic Resonance Encephalography (MREG) data with very high temporal resolution (100ms), and the spatiotemporal patterns that they obtained are much different in spatial extent and timing than the BOLD QPPs linked to infraslow electrical activity.

Global Signal

Global signal regression is a controversial topic (Power et al., 2017; Murphy and Fox 2016). Sustained motion-induced and respiratory-induced signal fluctuations are only removed by global signal regression, but it may also remove possible widespread neuronal co-activations, increase the spatial extent and strength of anti-correlations, and distort the variation structure (Saad et al., 2012). In this work, we have solely quantified individual differences in the fluctuation level of the global signal, and observed that global signal regression leads to more homogenous aspects of QPP across individuals.

A feature of the global signal is worth highlighting: its distribution is bimodal (**Fig. S12a**) and approximately the borderline between two modes matches the borderlines in Fig. 3e that separate mostly correlated QPPs from QPPs with strong anti-correlations.

Lastly note the rms values of global signal reported here are based on the average of the timeseries with our three additional preprocessing steps applied. These rms values are highly correlated (r:0.95) with rms values without any additional preprocessing steps named MGT (mean of grayordinate timeseries) in the HCP dataset (**Fig. S12b**).

Motion

Motion has complex effects on the MRI signal that are only partially compensated with correction strategies. While it seemed unlikely that the repetitive patterns detected with the QPP algorithm could arise from head motion, we used a subject group with very low motion in our original analysis. The

results were similar to previous studies of QPPs and suggest that motion is not a major contributor to the QPP. After this original analysis, the subject pool was expanded to include a much larger number of subjects with more typical levels of motion. The 470 subjects of this study were chosen based on an arbitrary threshold on FD (Fig. S1a) and neither of two FD metrics were significantly higher in individuals with the most-correlated QPP type relative to those with the anti-correlated type (Fig. S5). Based on these findings, the FD threshold can potentially be increased to include more subjects. Nevertheless, motion should be considered when evaluating differences in QPP metrics across groups. It seems likely that more motion could decrease the amplitude and frequency of QPP correlation, for example, as motion-related changes could mask the QPP.

Limitation and Future work

The QPP algorithm was initially developed to capture repeated large scale patterns of brain activity. Using this correlation-based approach on the whole brain is likely to identify the pattern with the strongest activity and largest spatial extent. Work in rodents that limits the algorithm to small sections of the brain (e.g., the subcortical grey matter) suggests that other, less prominent patterns may coexist with the QPP described in this manuscript (Majeed et al., 2011), an avenue that should be explored in future work. The current work focuses on characterizing the most representative QPP and how it varies across individuals. Note too that the present analysis focused on cortical areas, but subcortical regions also exhibit potentially interesting patterns in the QPP (Fig. 2) that we plan to further explore.

To achieve practical computation times while using the modified QPP method that examines every time point, analysis was performed on a parcel-wise basis for most of this work. Our preliminary analysis, based on 40 low movers, has shown that QPP type, correlation histogram and relation with the global signal, do not change when analyzed parcel-wise as opposed to voxel-wise. Also, as shown in Glasser et al., 2016b or Chen et al., 2015, parcel-wise analysis has the additional advantage of increasing the statistical significance. In our results, for instance, QPP correlation significantly increases. However, some of the fine details of the QPP are lost due to the spatial downsampling. For example, the propagation along the cortex observed by Majeed et al. 2009 and 2011 or even in this report (particularly evident in the videos) is difficult to detect in the parcel-wise QPP.

For the current analysis, all of the free parameters for the QPP analysis were kept constant across subjects. However, the outcomes suggest that some of these parameters should be optimized on an individual basis. For example, visual inspection of all 470 QPP1s shows that the full cycles are slightly different from 30 timepoints for some individuals (see **Fig. S13** for a typical and two extreme examples). As shown in Majeed et al., 2011, the QPP algorithm is robust in finding templates whose duration slightly deviates from a preset value, and qualitatively all the results presented in this work, such as QPP type and relation with global signal, seem robust in this regard as well, but systematically determining the optimal window-length for each individual is a goal of our future work.

The modified QPP algorithm uses all time points to avoid any potential biases. Nevertheless, it is clear from Fig. 1b that considerable redundancy results. A carefully-selected subset would ensure robust detection of the primary QPP while reducing the computation time. The selection of this subset will be explored in future work.

The origins of the QPPs remain poorly understood and are critical to understanding the neuro-physiological processes that are represented in MRI-based measurements of functional connectivity (FC). The spatially coherent fluctuations of the QPP certainly contribute to FC measurements, while the relatively long time scale and repetitive nature of the patterns is evidence that they are not directly tied to cognitive processing. To determine if QPPs were linked to the variations in correlation observed with sliding window techniques, we looked at phase amplitude coupling between infra-slow activity and higher frequencies (Thompson et al, 2014b), but found little evidence of a relationship. Further work showed that infra-slow electrical activity correlated with QPPs and higher frequency activity correlated more closely to sliding window BOLD correlation (Thompson et al, 2015), strong evidence that the QPPs and remaining BOLD signal have differing sensitivities to neural activity and do not reflect the same underlying events. The link between QPPs and infra-slow electrical activity suggests that QPPs are likely to reflect a distinct brain process that may itself be of interest, but at a minimum, QPPs are a source of non-cognitive BOLD fluctuations that can be removed as a nuisance signal like respiration or cardiac pulsation. Both the corrected BOLD FC maps and the QPP templates have the potential to provide new insight into the basic organization of the brain as well as neurological and psychiatric disorders.

Conclusion

This work provides the first assessment of the variability in individual QPPs and their relationship to global signal and physiological parameters. Improving the characterization of QPPs might provide further insight into the organization of dynamic brain activity, which in turn could underlie behavioral differences in the healthy population or connectivity changes in neurological and psychiatric disorders.

Acknowledgment

The authors thank Derek Smith, Anzar Abbas, and Dr. Savannah Cookson for their comments and Dr. Shiyang Chen and Dr. Jacob Billings for their very helpful discussions. We also thank Dr. Matt Bezdek, Dr. Wenju Pan, Dr. Garth Thompson, Amrit Kashyap, Prof. David Van Essen, Dr. Cesar Caballero-Gaudes, Dr. Bruce Crosson, and Alican Nalci for their one-time yet valuable comments. This work was funded by the NIH and NSF.

References

Majeed, W., Magnuson, M., Hasenkamp, W., Schwarb, H., Schumacher, E.H.H., Barsalou, L., Keilholz, S.D.D., 2011. Spatiotemporal dynamics of low frequency BOLD fluctuations in rats and humans. Neuroimage 54, 1140–1150. doi:10.1016/j.neuroimage.2010.08.030

Chang, C., Glover, G.H., 2010, Time-frequency dynamics of resting-state brain connectivity measured with fMRI, NeuroImage, 50:81-98

Allen, E.A., Damaraju, E., Plis, S.M., Erhardt, E.B., Eichele, T., Calhoun, V.D., 2012. Cerebral Cortex, 24:663-676. doi:10.10993/cercor/bhs352

Keilholz, S.D., Magnuson, M.E., Pan, W.J., Willis, M., Thompson, G.J., 2013. Dynamic properties of functional connectivity in the rodent. Brain Connectivity, 3:31-40. doi:10.1089/brain.2012.0115

Petridou, N., Caballero Gaudes, C., Dryden, I.L., Francis, S.T., Gowland, P.A., 2013. Periods of rest in fMRI contain individual spontaneous events which are related to slowly fluctuating spontatneous activity. Hum. Brain Mapp. 34:1319-1329. doi: 10.1002/hbm.21513

Caballero Gaudes, C., Petridou, N., Francis, S.T., Dryden, I.L., Gowland, P.A., 2013. Paradigm free mappign with sparse regression automatically detects single-trial functional magnetic resonance imaging blood oxygenation level dependent responses, Hum. Brain Mapp. 34:501-518

Liu, X., Duyn, J.H., 2013. Time-varying functional network information extracted from brief instances of spontaneous brain activity, Proc. Natl. Acad. Sci. USA, 110: 4392–4397

Chen, J.E., Chang, C., Greicius, M.D., Glover. G.H., 2015. Introducing co-activation pattern metrics to quantify spontaneous brain network dynamics. NeuroImage, 111, 476-488.

Kiviniemi, V., Wang, X., Korhonen, V., Keinanen, T., Tuovinen, T., Autio, J., LeVan, P., Keilholz, Sh., Zang, Y., Hennig., J., Nedergaard, M., 2016. Ultra-fast magnetic resonance encephalography of physiological brain activity - Glymphatic pulsation mechanisms? J. Cereb. Blood Flow Metab., 36, 1033-1045, doi:10.1177/0271678X15622047

Preti, M.G., Bolton, T.A.W., Van de Ville, D., 2016. The dynamic functional connectome: state-of-the-art and perspectives, Neuroimage, doi:10.1016/j.neuroimage.2016.12.061

Majeed, W., Magnuson, M., Keilholz, S.D., Majeed M.; Keilholz, S., W.M., 2009. Spatiotemporal Dynamics of Low Frequency Fluctuations in BOLD fMRI of the Rat. J Magn Reson Imag 30, 384–393. doi:10.1002/jmri.21848

Pan, W. J.J., Thompson, G.J., Magnuson, M.E., Jaeger, D., Keilholz, S., 2013. Infraslow LFP correlates to resting-state fMRI BOLD signals. Neuroimage 74, 288–297. doi:10.1016/j.neuroimage.2013.02.035

Thompson, G.J., Pan, W.J., Magnuson, M.E., Jaeger, D., Keilholz, S.D., 2014a. Quasi-periodic patterns (QPP): Large-scale dynamics in resting state fMRI that correlate with local infraslow electrical activity. Neuroimage 84, 1018–1031. doi:10.1016/j.neuroimage.2013.09.029

Thompson, G.J., Pan, W.J., Billings, J.C.W., Grooms, J.K.K., Shakil, S., Jaeger, D., Keilholz, S.D., 2014b. Phase-amplitude coupling and infraslow (<1 Hz) frequencies in the rat brain: relationship to resting state fMRI. Front Integr Neurosci 8, 41. doi:10.3389/fnint.2014.00041

Thompson, G.J., Pan, W.J., Keilholz, S.D., 2015. Different dynamic resting state fMRI patterns are linked to different frequencies of neural activity. J. Neurophysiol. 114, 114–24. doi:10.1152/jn.00235.2015

Keilholz, S.D., 2014. The Neural Basis of Time-Varying Resting-State Functional Connectivity. Brain Connectivity 4, 769-779. doi:10.1089/brain.2014.0250

Grooms, J.K., Thompson, G.J., Pan, W.J., Billings, J., Schumacher, E.H., Epstein, C.M., Keilholz, S.D., 2017. Infraslow EEG and dynamic resting state network activity. Brain Connectivity, doi:10.1089/brain.2017.0492

Keilholz, S.D., Pan, W.J., Billings, J., Nezafati, M., Shakil, S., 2016. Noise and non-neuronal contributions to the BOLD signal: application to and insights from animal studies. doi:10.1016/.neuroimage.2016.12.019

Van Essen, D.C., Smith, S.M., Barch, Deanna M.B., Behrens, T.E.J., Yacoub, E., Ugurbil, K., 2013. The WU-Minn Human Connectome Project: An Overview. NeuroImage, 80, 62-79.

Glasser, M., Smith, S.M., Marcus, D., Andersson, J.L.R., Auerbach, E.J., Behrens, T.E.J., Coalson, T.S., Harms, M.P., Jeninson, M., Moeller, S., Robinson, E.C., Sotiropoulos, S.N., Xu, J., Yacob, E., Ugurbil, K., Van Essen, D.C., 2016a. The Human Connectome Project's neuroimaging approach. Nature Neuroscience, 19, 1175-1187.

Power, J.D., Plitt, M., Laumann, T.O., Martin, A., 2017. Sources and implications of whole-brain fMRI signals in humans. NeuroImage, 146, 609-625.

Liu, T.T., Nalci, A., Falahpour, M., 2017. The global signal in fMRI: Nuisance or Information? NeuroImage 150, 213-229.

Chang, C., Glover, G.H., 2009. Effects of model-based physiological noise correction on default mode network anti-correlations and correlations. NeuroImage, 47, 1448-1459.

Birn, R.M., Smith, M.A., Jones, T.B., Bandettini, P.A., 2008. The respiration response function: The temporal dynamics of fMRI signal fluctuations related to changes in respiration. NeuroImage, 40, 644-654.

Birn, R.M., Diamond, J.B., Smith, M.A., Bandettini, P.A., 2006. Seperating respiratory-variation-related fluctuations from neuronal-activity-related fluctuations in fMRI, NeuroImage, 31: 1536-1548.

Glasser, M.F., Sotiropoulos, S.N., Wilson, J.A., Coalson, T.S., Fischl, B., Andersson, J.L., Xu, J., Jbabdi, S., Webster, M., Polimeni, J.R., Van Essen, D.C., Jenkinson, M., 2013. The minimal preprocessing pipeline for the Human Connectome Project. NeuroImage, 80, 105-124.

Power, J.D., Mitra, A., Laumann, T.O., Snyder, A.Z., Schlaggar, B.L., Peterson, S.E., 2014. Methods to detect, characterize, and remove motion artifact in resting state fMRI. NeuroImage, 84, 320-341

Glasser, M.F., Coalson, T.S., Robinson, E.C., Hacker, C.D., Harwell, J., Yacoub, E., Ugurbil, K., Andersson, J., Beckmann, C.F., Jenkinson, M., Smith, S.M., Van Essen, D.C., 2016b. A multi-modal parcellation of human cerebral cortex. Nature 536, 171–178. doi:10.1038/nature18933

Chang, C., Cunningham, J.P., Glover, G.H., 2009. Influence of heart rate on the BOLD signal: The cardiac response function. NeuroImage, 44, 857-869.

Wong, C.W., Olafsson, V., Tal, O., Liu, T.T., 2013. The amplitude of the resting-state fMRI global signal in related to EEG vigilance measures. NeuroImage, 83:983-90. doi:10.101.neuroimage.2013.07.057

Belloy, M., Naeyaert, M., Keliris, G., Abbas, A., Keilholz, S., Van Der Linden, A., Verhoye, M., 2017. Dynamic resting state fMRI in mice: detection of Quasi-Periodic Patterns, In: Proceeding of the International Soc. Magn. Reson. Med. p.0961.

Magnuson, M., Majeed, W., Keilholz, S.D., Functional connectivity in blood oxygenation level-dependent and cerebral blood volume-weighted resting state functional magnetic resonance imaging in the rat brain, 2010. J Magn. Reson. Imaging 32:584-592. doi: 10.1002/jmri.22295.

Abbas, A., Langley, J., Howell, L., Keilholz, S., 2016a. Quasiperiodic patterns vary in frequency between anesthetized and awake monkeys, Resting State Brain Connectivity Biennial Conference, p.141.

Buckner, R.L., Andrews-Hanna, J.R., Schacter, D.L., 2008. The brain's default network: anatomy, function, and relevance to disease. Ann. N. Y. Acad. Sci. 1124, 1-38.

Fox, M.D., Snyder, A.Z., Vincent, J.L., Corbetta, M., Van Essen, D.C., Raichle, M.E., 2005. The human brain is intrinsically organized into dynamic, anticorrelated functional networks. Proc Natl Acad Sci U S A 102: 9673-978. doi:10.1073/pnas.0504136102.

Murphy, K., Fox, M.D., 2016. Towards a consensus regarding global signal regression for resting state functional connectivity MRI. NeuroImage. http://dx.doi.org/10.1016/.neuroimage.2016.11.052

Rosenberg, M.D., Finn, E.S., Scheinost, D., Papademetris, X., Shen, X., Constable, R.T., Chun, M.M., A neuromarker of sustained attention from whole-brain functional connectivity. Nature Neuroscience, 19, 165-171. doi:10.1038/nn.4179

Tavor, I., Parker Jones, O., Mars, R.B., Smith, S.S., Behrens, T.R., Jbabdi, S., 2016. Task-free MRI predicts individual differences in brain activity during task performance. Science, 352, 216-220.

Smith, S.M., Nichols, T.E., Vidaurre, D., Winkler, A.M., Behrens, T.E.J., Glasser, M.F., Ugurbil, K., Barch, D.M., Van Essen, D.C., Miller, K.L., 2015. A positive-negative mode of population covariation links brain connectivity, demographics and behavior. Nat Neurosci, 18:1565–1567.

Cole, M.W., Bassett, D.S., Power, J.D., Braver, T.S., Petersen, S.E., 2014. Intrinsic and task-evoked network architectures of the human brain. Neuron, 83: 238–251

Schultz, D.H., and Cole, M.W., 2016. Higher intelligence is associated with less task-related brain network reconfiguration. J. Neurosci, 36:8551–8561.

Abbas, A., Majeed, W., Thompspn, G., Keilholz, S.D., 2016b. Phase of quasi-periodic patterns in the brain predicts performance on psychomotor vigilance task in humans, In: Proceeding of the International Soc. Magn. Reson. Med. p. 1192.

Broyd, S.J., Demanuele, C., Debener, S., Helps, S.K., James, C.J., Sonuga-Barke, E.J., 2009. Default-mode brain dysfunction in mental disorders: a systemic review. Neurosci Beiobehav Rev, 33, 279-296

Moore, C.I., Cao, R., 2008, The hemo-neuroal hypothesis: on the rold of blood flow in information processing. J Neurophysiol 99:2035:2047. doi:10.1152/jn.01366.2006

Murphy, K., Birn, R.M., Bandettini, P.A., 2013. Resting-state fMRI confounds and cleanup. 80, 349-359.

Vlemincx, E., Abelson, J. L., Lehrer, P. M., Davenport, P., W., Van Diest, I., Van den Bergh, O., 2013a, Respiratory variability and sighing: A psychophysiological reset model. Biologiical Psychology, 93:24-32. doi.10.1016/j.biopsycho.2012.12.001

Vlemincx, E., Vigo, D., Vansteenwegen., D., Van den Bergh, O., Van Diest, I., 2013b. Do not worry, be mindful: Effects of induced worry and mindfulness on respiratory variability in a nonanxious population. International Journal of Psychophysiology, 87:147-151. doi.10.1016/j-ijpsycho.2012.12.002

Saad, Z.S., Gotts, S.J., Murphy, K., Chen, G., Jo, H.J., Martin, A., Cox, R.W., 2012. Trouble at rest: how correlation patterns and group differences become distorted after global signal regression. Brain Connect 2, 25-32

Burgess, G.C., Kandala, S., Nolan D., Laumann, T.O., Power, J.D., Adeyemo, B., Harms, M.P., Petersen, S.E., Barch, D.M., 2016. Evaluation of denoising strategies to address motion-correlated artifacts in resting-state functional magnetic resonance imaging data from Human Connectome Project. Brain Connectivity, 6, 669:680. doi:10.1089/brain.2016.0435

Siegel, J.S., Mitra, A., Laumann, T.O., Seitzman, B.A., Raichle M., Corbetta M., Snyder, A.Z., 2016. Data Quality Influences Observed Links Between Functional Connectivity and Behavior. Cereb. Cortex. http://dx.doi.org/10.1093/cercor/bhw253.

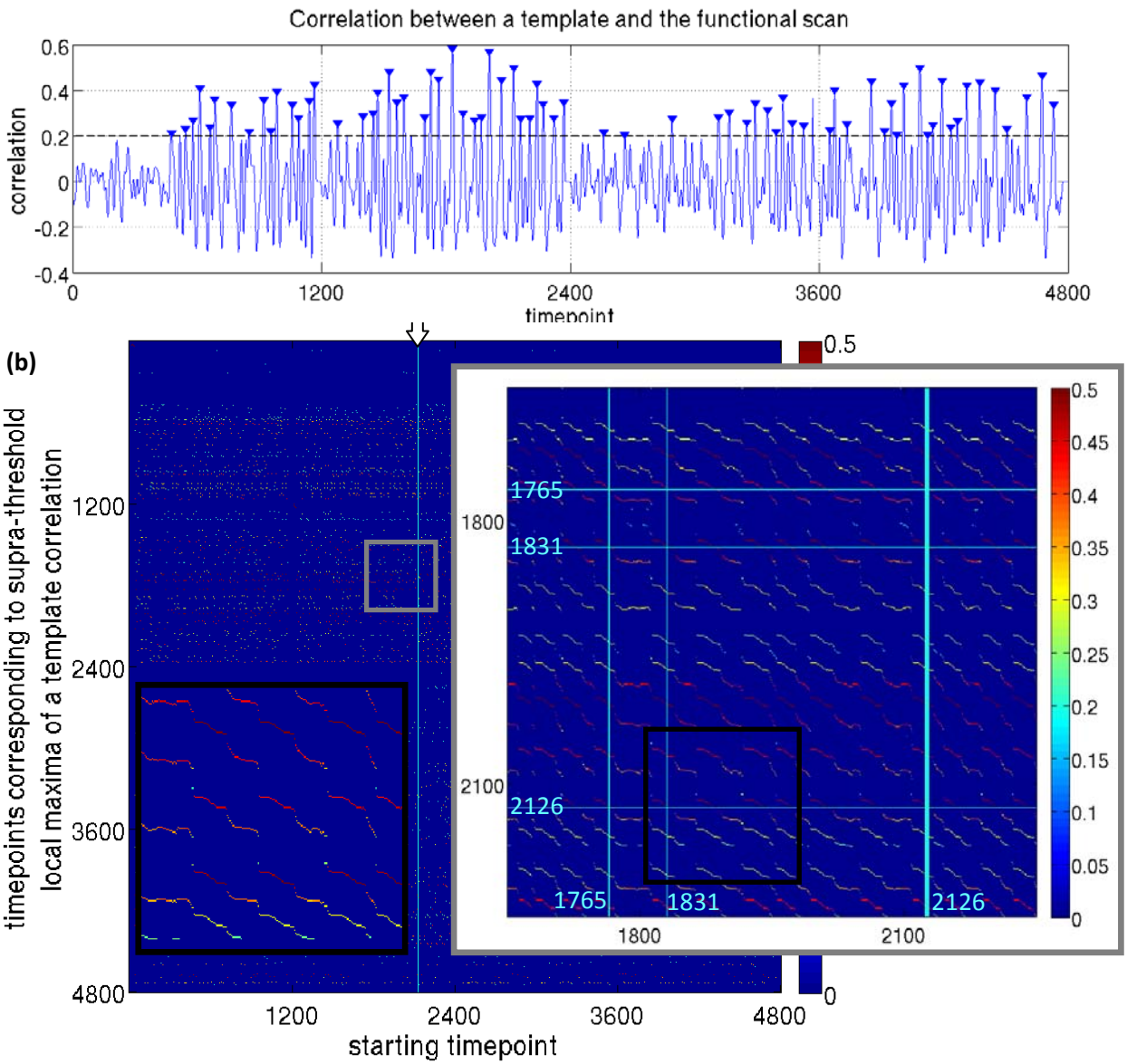

Fig. 1. (a) Correlation between a template corresponding to a single starting timepoint and the entire scan for one individual. **(b)** Timepoints corresponding to supra-threshold local maxima of a template correlation timecourse (e.g., marked in Fig1a) plotted in the vertical axis for each starting time point, with the value of correlation is indicated by color. When all timepoints are considered as starting timepoints, considerable redundancy results: (i) sequential starting timepoints detect different phases of the same template (black inset), and (ii) starting timepoints which are ~30 timepoints apart are essentially part of the same template; for instance, Fig. 1a corresponds to the starting timepoint 2126 (**thick** vertical cyan line) and 1765 and 1831 are among supra-threshold maxima (and the corresponding template is the average of the segments of scan starting at those maxima after convergence of the algorithm), when 1765 is the starting timepoint, 1831 and 2126 are among supra-threshold maxima and when 1831 is the starting time point, 1765 and 2126 are among supra-threshold maxima.

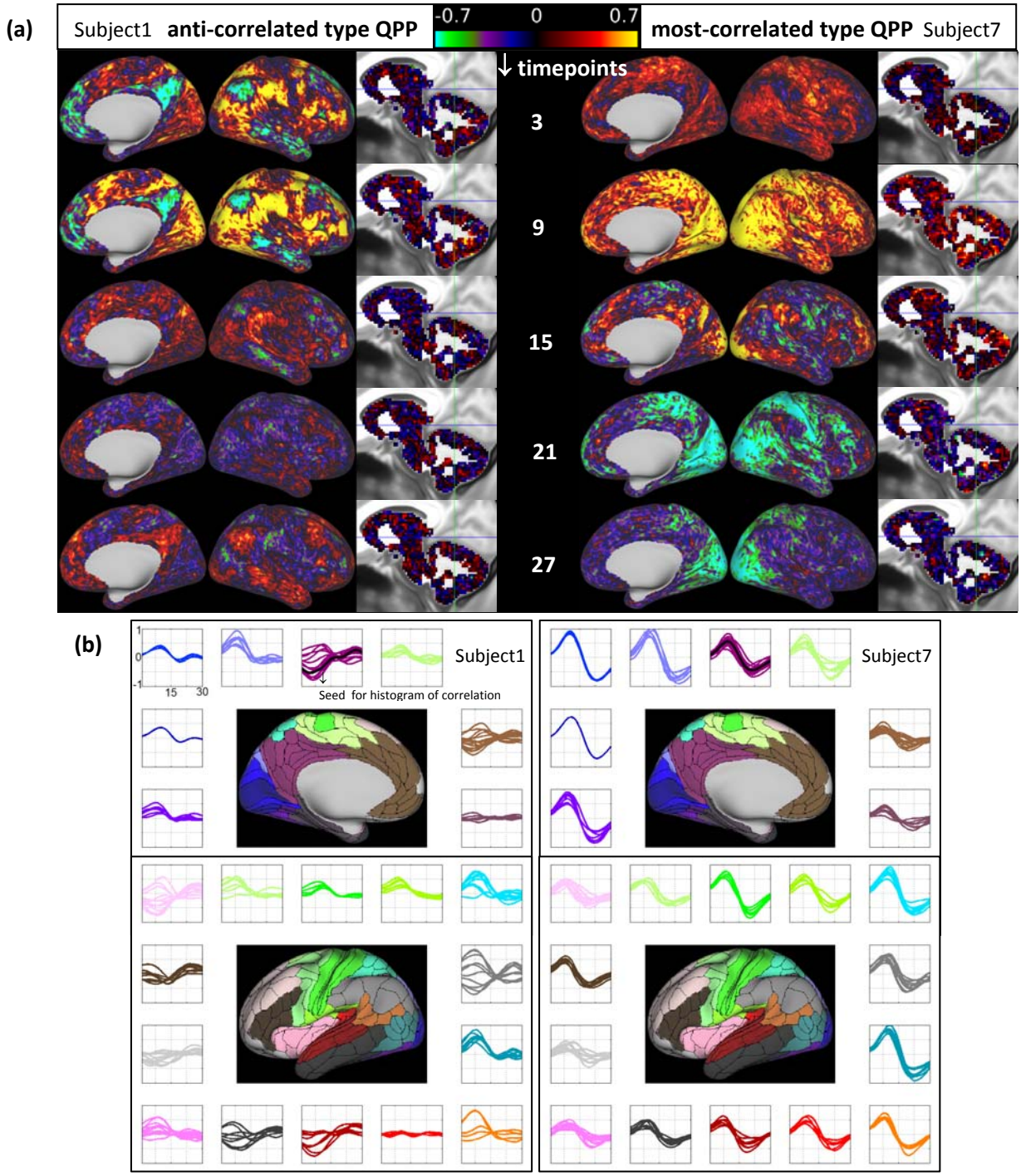

Fig. 2. (a) QPPs from two representative subjects: One exhibits anti-correlated activity between DMN and non-DMN areas (anti-correlated type QPP) and the other exhibits correlated activity in most areas, with only a few time points showing anti-correlation (most-correlated type QPP). **(b)** The same subjects shown in parcel-wise format. Subplots showing the signal in the QPP template for each parcel at each time point, with each parcel residing in one of 22 subplots corresponding to Glasser's 22 Networks (color-coded).

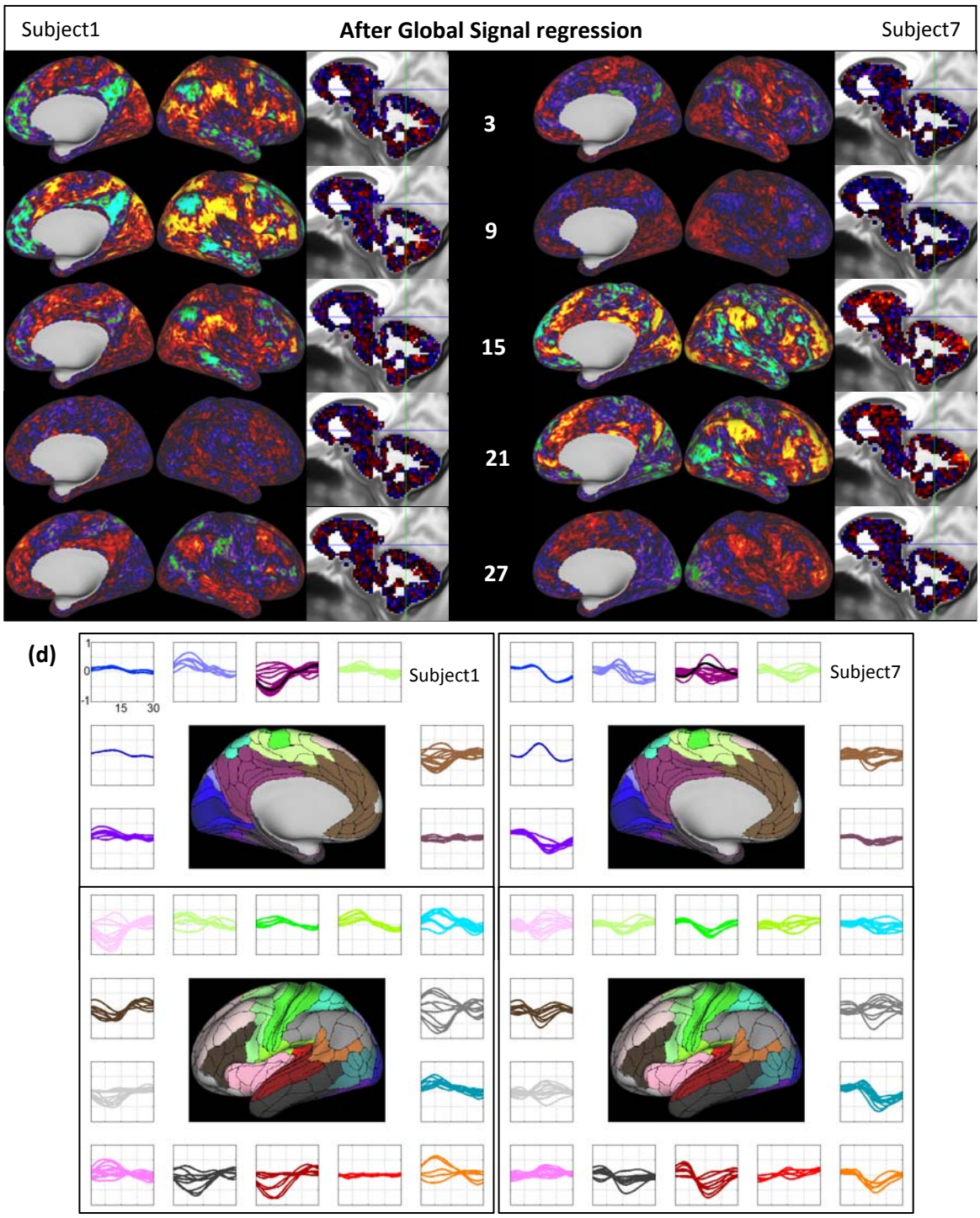

Fig. 2. (c) and **(d)** the same as (a) and (b) after global signal regression. After global signal regression, both subjects exhibit anti-correlation between the DMN and TPN in their templates.

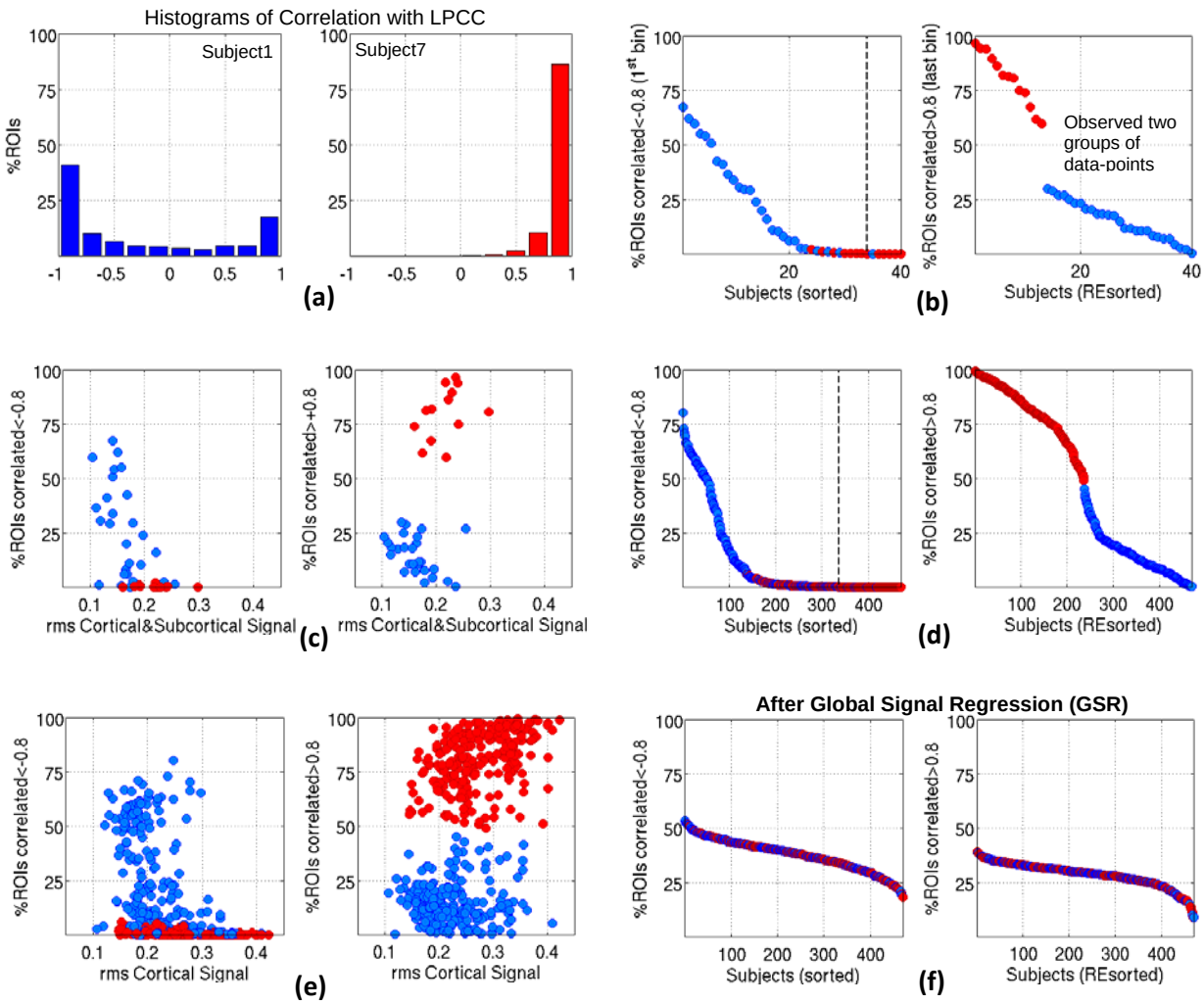

Fig. 3. (a) histograms of correlations with LPCC for the two QPPs shown in Fig. 2a and b. **(b)** Left plot: 40 low movers sorted based on the value of the first bin of their histogram of correlation (%ROIs correlated<-0.8), with the dashed line indicating when zero is reached. Right plot: 40 low movers are **RE**sorted based on the value of the last bin of their histogram of correlation (%ROIs correlated>0.8). Two groups of data-points are evident. **(c)** %ROIs with strong negative and positive correlations shown in (b) are plotted against rms of the global signal. **(d) and (e)** are similar to (b) and (c), respectively, for 470 low-moderate movers and show a similar separation into two groups. **(f)** Sorted histograms similar to (d) but with global signal regression performed before QPP analyses. All 470 subjects show substantial anti-correlation within their QPPs.

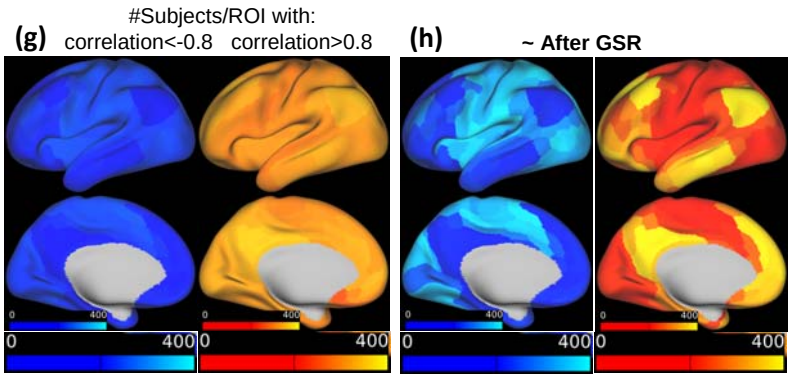

Fig. 3. (g) Number of subjects with strong negative and positive correlations per each ROI. Most ROIs with strong anti-correlation belong to non-DMN networks and most ROIs with strong correlation belong to DMN, **(h)** Similar to **(g)** but after global signal regression. Strong correlation and anti-correlation are much more localized.

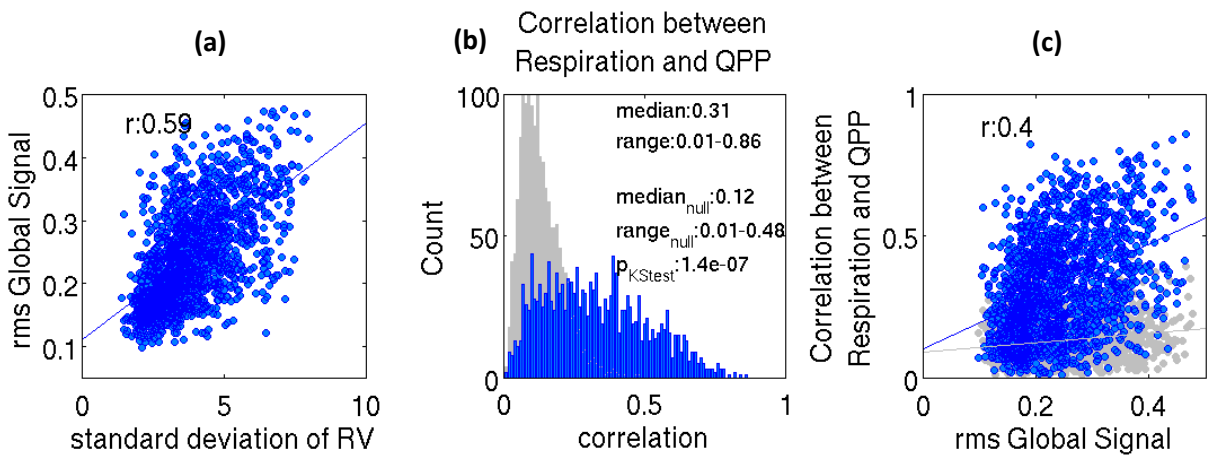

Fig. 4 (a) rms of global signal is correlated with standard deviation of respiratory variation (4×403 datapoints correspond to four scans of 403 individuals included for RV analysis)**. (b)** The distribution of cross-correlation between respiratory-induced signal fluctuations (RV⊗RRF) and QPP occurrence (QPP1⊗C1@ROI1$_{RV}$), as compared to a null distribution made from phase-randomized time series (null in gray). **(c)** Relation with rms of global signal. QPP occurrence weakly yet significantly coincides with respiratory-induced signal fluctuations and the higher the rms of the global signal, the stronger this coincidence.

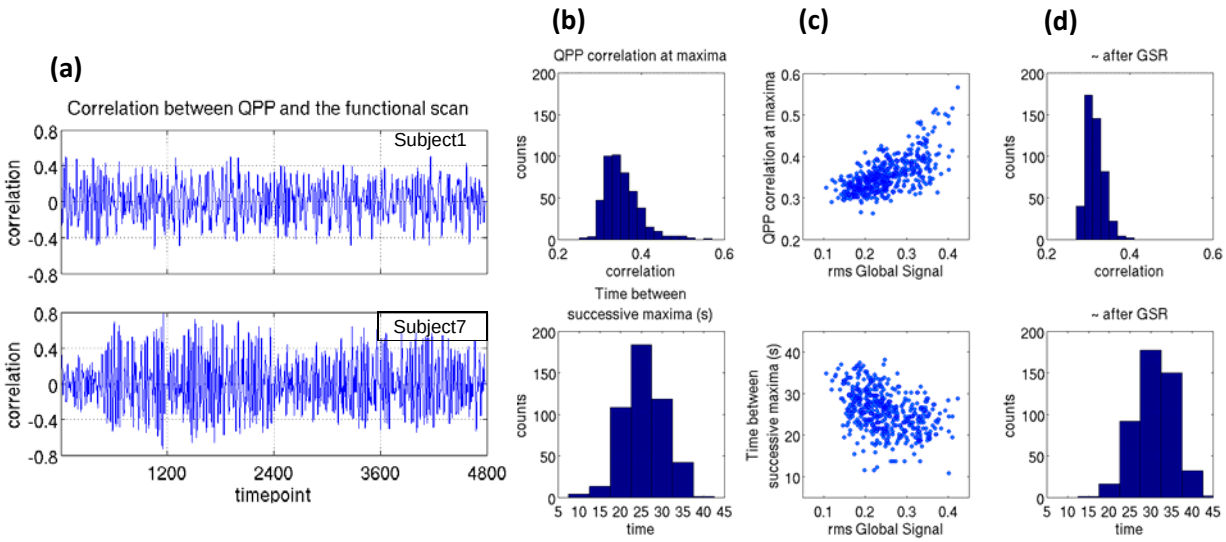

Fig. 5. (a) The time course of correlation between QPP and the functional scan for the same two representative subjects in Fig 2a and 3a. The median of QPP correlation at supra-threshold local maxima, which describes the strength of the QPP, is 0.31 for Subject 1 and 0.36 for Subject7. The median of the time between successive maxima, which describes how often the pattern occurs, is 30s and 22s, respectively (the sum of all QPP correlation values at supra-threshold local maxima, which depends on both the strength of the pattern and how often it occurs, is 32 for Subject 1 and 57 for Subject 7). As observed at the group level, in these two representative subjects, the QPP occurs more often and is more strongly correlated in the subject with higher global signal (Subject 7). **(b)** For all 470 subjects, histograms describe the median of QPP correlation at supra-threshold local maxima (top, median:0.35, range:0.26-0.57) and time between successive supra-threshold local maxima (bottom, median:26s, range:11-38s). **(c)** values of (b) versus rms of global signal; a higher rms of the global signal (likely the most-correlated QPP type) corresponds to higher correlation and periodicity, **(d)** same as (c) after global signal regression; QPPs' correlation and periodicity decrease (correlation has median of 0.31 and range of 0.27-0.4, and time difference has median of 32s and range of 15-44s).

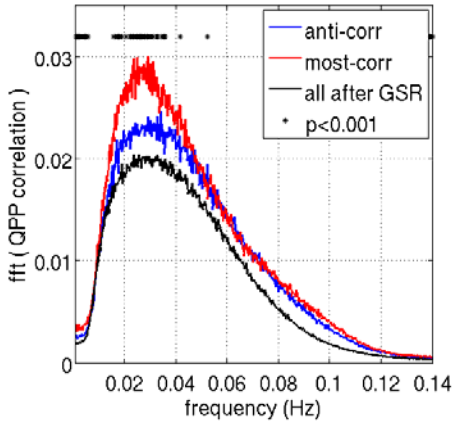

Fig. 6. The averaged Fourier transform of QPP correlation across all subjects exhibits a broad peak at 0.02-0.04 Hz, qualitative evidence of the quasi-periodic nature of the pattern. The peak is significantly different between the two QPP types or when comparing before and after global signal regression.

(a)

		Day1	
		anti	most
Day2	Anti	178	95
	most	67	130

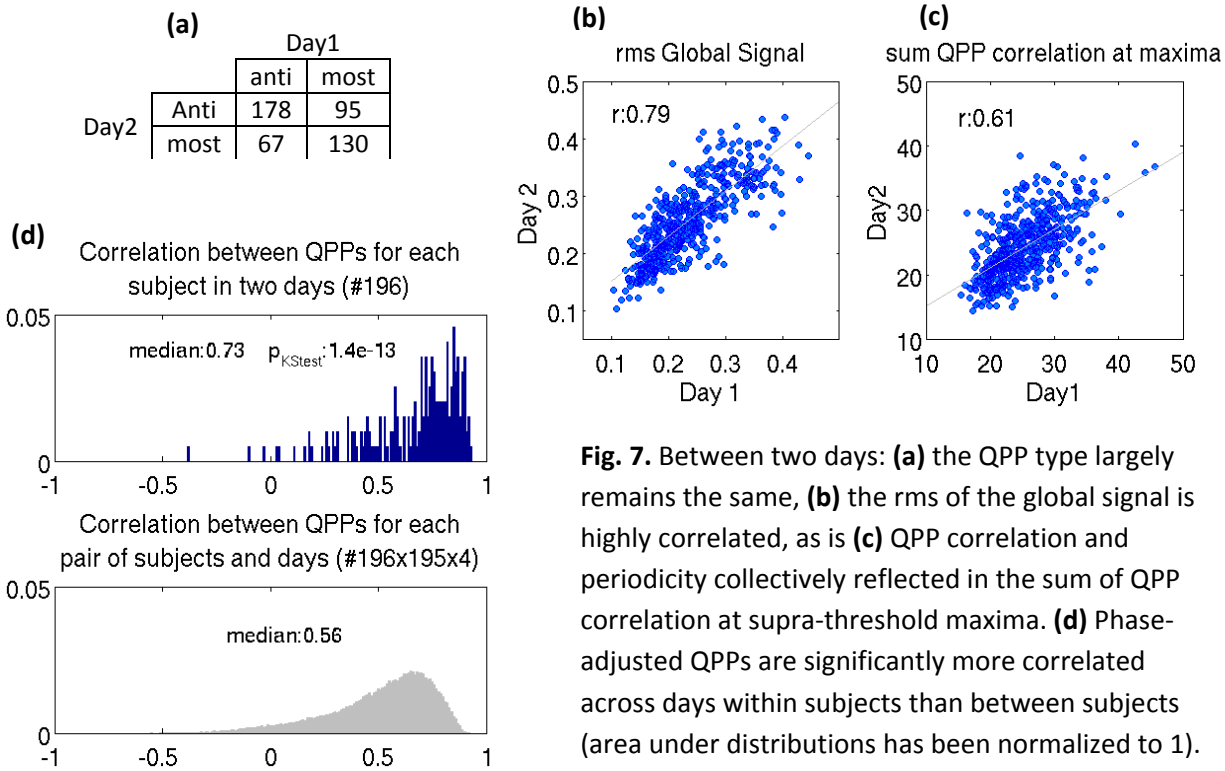

Fig. 7. Between two days: **(a)** the QPP type largely remains the same, **(b)** the rms of the global signal is highly correlated, as is **(c)** QPP correlation and periodicity collectively reflected in the sum of QPP correlation at supra-threshold maxima. **(d)** Phase-adjusted QPPs are significantly more correlated across days within subjects than between subjects (area under distributions has been normalized to 1).